VIP Water Splitting Very Important Paper

International Edition: DOI: 10.1002/anie.201508024
German Edition: DOI: 10.1002/ange.201508024

Boosting Photocatalytic Water Splitting: Interfacial Charge Polarization in Atomically Controlled Core–Shell Cocatalysts

*Song Bai, Li Yang, Chunlei Wang, Yue Lin, Junling Lu, Jun Jiang, and Yujie Xiong**

Abstract: *Platinum is a commonly used cocatalyst for improved charge separation and surface reactions in photocatalytic water splitting. It is envisioned that its practical applications can be facilitated by further reducing the material cost and improving the efficacy of Pt cocatalysts. In this direction, the use of atomically controlled Pd@Pt quasi-core–shell cocatalysts in combination with TiO_2 as a model semiconductor is described. As demonstrated experimentally, the electron trapping necessary for charge separation is substantially promoted by combining a Schottky junction with interfacial charge polarization, enabled by the three-atom-thick Pt shell. Meanwhile, the increase in electron density and lattice strain would significantly enhance the adsorption of H_2O onto Pt surface. Taken together, the improved charge separation and molecular activation dramatically boost the overall efficiency of photocatalytic water splitting.*

Sunlight-driven water splitting provides a promising approach to transform solar energy into hydrogen fuel.[1–3] In the process of photocatalysis, electron–hole separation and surface reactions are two of the three steps that hold the key to achieving high quantum efficiencies. The use of cocatalysts that not only promote electron–hole separation but also provide active sites for H_2O adsorption and activation opens the possibility to improve the overall photocatalytic efficiency.[4–6] Among various cocatalysts, platinum has been demonstrated to be a highly active cocatalyst material for water splitting through forming a Schottky junction and providing an active surface; however, high material costs would impede its practical applications.

Towards the development of high-performance, low-cost photocatalysts, reducing the Pt usage is always the ultimate goal for cocatalyst design. It would be ideal if the efficacy of the cocatalyst could concomitantly be further enhanced in terms of charge separation and surface reactions. Most recently, we have invented a Pt–Pd–graphene stack structure for the electrocatalytic hydrogen evolution reaction (HER).[7] The 0.8 nm thick Pt shell enables the accumulation of negative charges on the Pt surface through interfacial charge polarization, promoting the HER process. Naturally, we were intrigued whether such an interfacial charge polarization could be implemented in the cocatalyst design towards improved photocatalytic water splitting. If possible, we would only need to use a few atomic layers of Pt as the cocatalyst while concomitantly further improving the water-splitting performance.

Herein, we report the development of atomically controlled Pd@Pt core–shell cocatalysts and their implementation in combination with a commonly used n-type semiconductor, namely anatase TiO_2. Enabled by the three-atom-thick Pt shell, electron trapping by the Schottky junction can be promoted by the charge polarization occurring at the interface of Pd and Pt, which facilitates charge separation and prolongs the carrier lifetime. Meanwhile, the increased electron density at the Pt surface, together with the lattice strain resulting from the ultrathin coating, enhances the adsorption of reactive H_2O molecules onto the Pt surface. As a result, the efficiency of photocatalytic water splitting has been remarkably improved by a factor of up to 322 compared to that of bare TiO_2 and by a factor of 8.2 compared to that of TiO_2–Pt hybrid structures with a comparable Pt{100} surface structure.

For our proof-of-concept studies, we used anatase TiO_2 nanosheets as a model semiconductor, which were synthesized according to a literature procedure.[8] As shown in the Supporting Information, Figure S1, the nanosheets with an edge length of approximately 200 nm and a thickness of 6–9 nm display (001) faces on flat surfaces. Taking advantage of the large flat surfaces, we could readily assemble pre-synthesized Pd nanocubes (which are covered by {100} facets)[9] on the TiO_2 nanosheets and anneal their interfaces through a hydrothermal process (see Figure S2). As indicated by Figure S3, the Pd nanocubes with an edge length of approximately 12 nm have been sparsely distributed over the TiO_2 nanosheets (resulting in TiO_2–Pd). This TiO_2–Pd hybrid structure is further coated with Pt atoms through a Pt precursor reduction, forming the TiO_2–Pd@Pt samples with tunable Pt thickness (Figure S2). Unlike in previously reported approaches,[10–12] the formation of a Schottky junction between TiO_2 and Pd naturally leads to the accumulation of electrons on the Pd surface to designate the Pd surface as the specific site for Pt reduction and deposition. As such, the Pt atoms can be selectively deposited on the Pd nanocubes with atomic precision. We specifically refer to this Pd@Pt configuration as a "quasi-core–shell structure", as only five faces of a Pd nanocube are covered by Pt while the other one is in intimate contact with TiO_2 (see Figure S4).

[*] Dr. S. Bai,[+] L. Yang,[+] C. Wang,[+] Dr. Y. Lin, Prof. J. Lu, Prof. J. Jiang, Prof. Y. Xiong
Hefei National Laboratory for Physical Sciences at the Microscale
iChEM (Collaborative Innovation Center of Chemistry for Energy Materials), Hefei Science Center (CAS) and School of Chemistry and Materials Science
University of Science and Technology of China
Hefei, Anhui 230026 (P. R. China)
E-mail: yjxiong@ustc.edu.cn

[+] These authors contributed equally to this work.

Supporting information for this article is available on the WWW under http://dx.doi.org/10.1002/anie.201508024.

Transmission electron microscopy (TEM) and scanning TEM (STEM) images of the sample with ultrathin Pt shells are shown in Figure 1a and 1b. The cubic nanocrystals

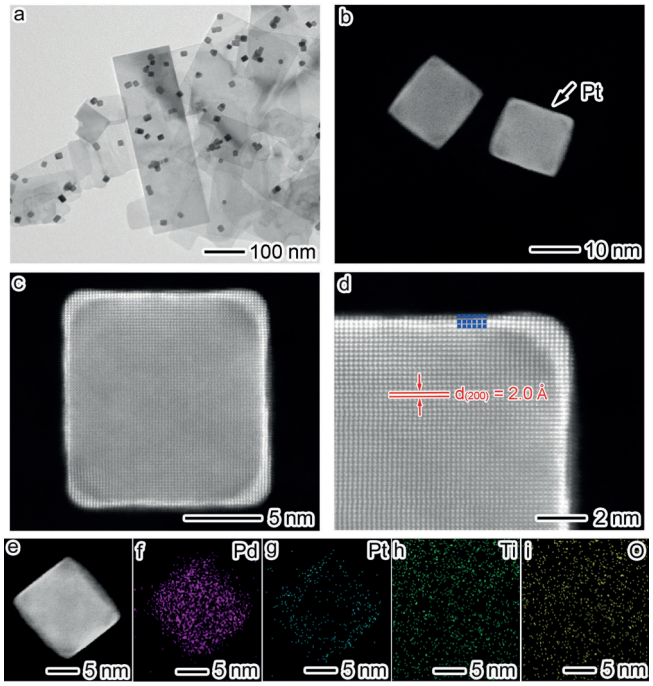

Figure 1. a) TEM image of a TiO_2–Pd@Pt_{3L} sample. b) Low-magnification, c) high-magnification, and d) atomic-resolution HAADF-STEM images of the Pd@Pt_{3L} quasi-core–shell nanostructures supported on TiO_2 nanosheets. e–i) STEM image and EDS mapping profiles of a single Pd@Pt_{3L} quasi-core–shell nanostructure on a TiO_2 nanosheet showing the Pd, Pt, Ti, and O distributions.

supported on the TiO_2 nanosheets have an average edge length of 13.2 nm, which is 1.2 nm greater than that of the original Pd nanocubes (Figure S5). This finding indicates that the Pt shell has a thickness of about 0.6 nm on average, which corresponds to three atomic layers according to the lattice constant. This argument is further supported by the aberration-corrected high-angle annular dark-field STEM (HAADF-STEM) images taken from an individual quasi-core–shell nanocube (Figure 1c,d). As Pt and Pd have significantly different atomic numbers, the images show a high contrast between the Pt shell and the Pd core so that the number of Pt atomic layers could be estimated to be three. Both the Pd core and the Pt shell are bounded by {100} facets as indicated by the lattice fringes. More statistical data were obtained by chemical composition measurements on the entire sample by inductively coupled plasma mass spectrometry (ICP-MS). As shown in Table S1, the atomic ratio of Pd to Pt determined by ICP-MS is consistent with three atomic layers. Therefore, we can safely conclude that the average number of Pt atomic layers is three (TiO_2–Pd@Pt_{3L}). The sample was further characterized by STEM and energy-dispersive spectroscopy (EDS) mapping analyses (Figure 1e–i), further confirming the quasi-core–shell structure supported on a TiO_2 nanosheet. The chemical compositions and crystal phases were confirmed by X-ray diffraction (XRD; Figure S6).

The Pt shell thickness could be readily tailored by altering the TiO_2–Pd hybrid/Pt precursor ratio during the synthesis. TEM images and EDS mapping profiles for another typical sample with an average of ten Pt atomic layers (TiO_2–Pd@Pt_{10L}) are shown in Figures S7 and S8. In particular, the HAADF-STEM results are in good agreement with the nanocrystal dimensions and ICP-MS measurements (see Table S1), unambiguously demonstrating the presence of ten atomic layers in the shells. The ability to control the shell thickness with atomic precision allows for investigating the impact of interfacial charge polarization on photocatalysis. To better assess the role of the Pd–Pt interface, we prepare a reference sample by depositing pure Pt nanocubes (with an edge length comparable to that of TiO_2–Pd@Pt_{3L}) on TiO_2 nanosheets as shown in Figure S9 (TiO_2–Pt). As illustrated in Table S1, all of the samples should have roughly the same number of cocatalyst nanocrystals supported on the TiO_2 nanosheets, according to the molar ratio of Pd/Pt to TiO_2 by taking the dimension changes of the metal nanocrystals into account. Such a consistency sets up a platform for reliably comparing their performance in terms of charge separation and surface reactions.

Figure 2a shows the photocurrents versus time (*I*–*t*) curves of all of the samples. Their photocurrents turn out to be in the order of bare TiO_2 < TiO_2–Pd < TiO_2–Pt < TiO_2–Pd@Pt_{10L} < TiO_2–Pd@Pt_{3L}. Given that the samples have comparable capabilities in terms of light absorption at < 400 nm (Figure S10), this result suggests that the use of quasi-core–shell cocatalysts leads to more efficient electron–hole separation. The efficiency of the charge separation increases as the thickness of the Pt shell decreases. Note that Pt has a higher work function than Pd (5.77 eV vs. 5.12 eV; see Figure S12), so that the TiO_2–Pt Schottky junction can better trap photoexcited electrons than a TiO_2–Pd junction.[4] In a complementary measurement, we collected photoluminescence (PL) emission spectra (Figure S11), which indicated that electron–hole recombination can be better suppressed by the Pd@Pt_{3L} cocatalyst. This finding was further confirmed by transient open-circuit voltage decay (OCVD) measurements (Figure 2b), which can be used to resolve charge kinetics.[13–15] As expected, the average lifetimes of the carriers were substantially prolonged by the quasi-core–shell cocatalyst design (see Figure 2c), and they follow the same sequence as the photocurrents: bare TiO_2 < TiO_2–Pd < TiO_2–Pt < TiO_2–Pd@Pt_{10L} < TiO_2–Pd@Pt_{3L}.

Having confirmed the charge-separation properties of these materials, we further investigated their performance in photocatalytic water splitting without the use of any sacrificial agents. Figure 2d summarizes the hydrogen production rates (for the hydrogen production rates per unit surface area of the metal cocatalysts, see Table S2). TiO_2–Pd@Pt_{3L} achieved an impressive value of greater than 600 μmol g_{cat}^{-1} h^{-1} at a low Pt usage (less than 0.9 mol% of the overall catalyst despite the ultrathin nature of the TiO_2 nanosheets). The hydrogen production rates follow the same order as the photocurrents, which reflects the importance of charge separation to the entire photocatalytic process. However, the difference

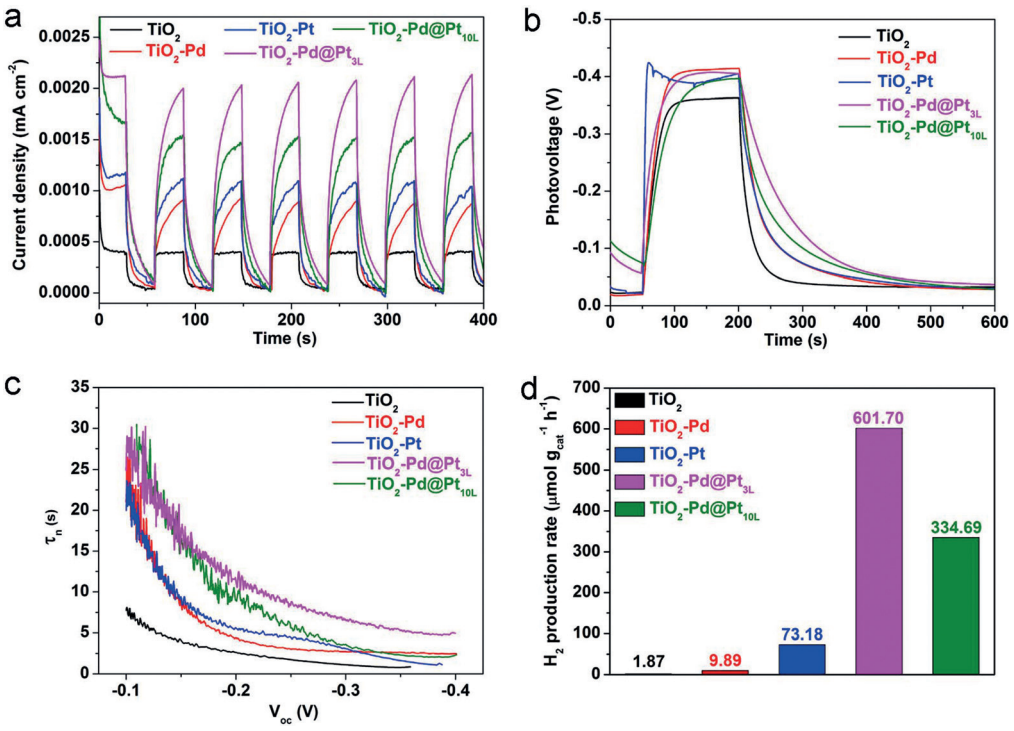

Figure 2. a) *I–t* curves of TiO_2–Pd@Pt_{3L} and TiO_2–Pd@Pt_{10L} in comparison with those of bare TiO_2 nanosheets, TiO_2–Pd, and TiO_2–Pt hybrid structures under UV light irradiation ($\lambda < 400$ nm, 2.7 mW cm^{-2}) at a bias potential of 0 V vs. Ag/AgCl. b) Transient OCVD measurements after exposure to UV light. c) Average lifetimes of the photogenerated carriers (τ_n) obtained from the OCVD measurements. d) Photocatalytic H_2 evolution from water with the samples as catalysts under the same irradiation conditions.

between TiO_2–Pt and TiO_2–Pd@Pt appears to be significantly larger in the photocatalytic performance. The activity of TiO_2–Pd@Pt_{3L} is 8.2 times higher than that of TiO_2–Pt although both possess a Pt{100} surface for hydrogen production. Therefore, the quasi-core–shell structure of the cocatalyst should also have altered the molecular adsorption and activation properties of the Pt{100} surface in addition to facilitating charge separation, which leads to the overall improvement. The large performance difference between TiO_2–Pt and TiO_2–Pd is mainly caused by the higher activity of Pt surfaces in water splitting.[4] The samples show stable catalytic activities in the water splitting reaction (Figure S13), as the quasi-core–shell cocatalysts were well maintained on the TiO_2 nanosheets after the reaction (Figure S14).

To understand the mechanism behind this process, we employed first-principles simulations[16] to examine the Pt thickness dependent behavior. We first assessed the role of the quasi-core–shell structures in charge separation by analyzing the differential charge densities between Pd@Pt hybrid structures and their isolated components. Driven by the different work functions of Pd and Pt, an electron migration across the interface from Pd to Pt will equilibrate their electron Fermi distributions. As indicated by the differential charge density (Figure S15), a certain number of electrons can be accumulated on the exposed Pt surface. This electron accumulation effect dramatically decays with an increase in Pt shell thickness, and nearly vanishes as the thickness reaches four atomic layers (see Table S3).

The thickness-dependent charge accumulation was experimentally confirmed by two characterization techniques. First, we employed CO as a probe molecule to resolve the electron density of the Pt surface. At higher electron densities, a CO molecule chemisorbed onto the Pt surface will accept additional electrons into its antibonding orbital, which thus reduces the vibrational frequency of CO.[17] Experimentally, CO chemisorption can be examined in situ by diffuse-reflectance infrared Fourier transform spectroscopy (DRIFTS) as outlined in Figure 3a. As Pt is deposited on the Pd nanocubes to form Pd@Pt quasi-core–shell structures, the vibrational peaks for linear and bridged CO on Pd at 2059.1 and 1926.0 cm^{-1}, respectively, disappeared. Instead, the peaks corresponding to CO chemisorption on Pt arise as the Pt shell reaches a thickness of three atomic layers (TiO_2–Pd@Pt_{3L}): 2088.5 cm^{-1} for linear CO and

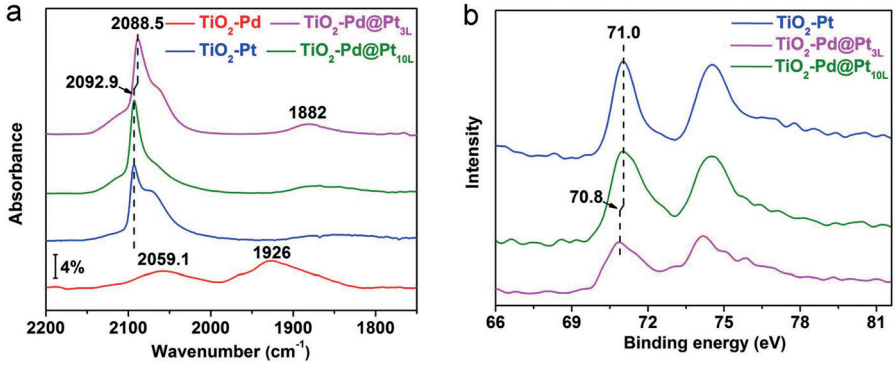

Figure 3. a) CO chemisorption DRIFTS spectra and b) XPS Pt 4f high-resolution spectra of TiO_2–Pd@Pt_{3L} and TiO_2–Pd@Pt_{10L} and TiO_2–Pt and/or TiO_2–Pd hybrid structures for comparison.

1882.0 cm^{-1} for bridged CO.[18] Compared with Pt nanocubes supported on TiO_2 ($\upsilon_{CO\ linear} = 2092.9\ cm^{-1}$), the vibrational frequency for linear CO on TiO_2–Pd@Pt_{3L} is 4.4 cm^{-1} lower, indicating the higher electron density of the Pt surface on TiO_2–Pd@Pt_{3L}. As the Pt shell thickness is increased to ten layers, the effect of interfacial polarization on the Pt surface is reduced to nearly zero, and the same vibrational frequency as for TiO_2–Pt is thus observed.

The increase in electron density should also shift the X-ray photoelectron spectroscopy (XPS) peaks for Pt 4f to lower binding energies. We thus collected XPS Pt 4f spectra for the Pt-based samples (Figure 3b). The Pt $4f_{7/2}$ peak for zero valence is located at 71.0 eV,[19] as shown for TiO_2–Pt. In contrast, the Pt $4f_{7/2}$ binding energy for TiO_2–Pd@Pt_{3L} is 0.2 eV lower, indicating the higher electron density of the Pt surface. Similarly to the CO chemisorption DRIFTS measurement, TiO_2–Pd@Pt_{10L} shows the same Pt binding energy as TiO_2–Pt, as the Pt surface does not benefit from a distinct interfacial polarization effect. The electron accumulation on the Pt surface was also supported by metal-selective deposition experiments (Figure S16).

The theoretical and experimental results clearly describe the interfacial behavior of Pd@Pt quasi-core–shell structures in the neutral state. In a photocatalytic process, once the supporting TiO_2 nanosheets have been photoexcited, the photogenerated electrons will be transferred to Pd because of the TiO_2–Pd Schottky junction. The charge accumulation associated with Pd–Pt interfacial polarization serves as the driving force for the photogenerated electrons to migrate from the Pd to Pt surface. As a result, the charge separation in the entire material system can be improved. Our simulation indicates that the addition of electrons to Pd will reduce the dependence of the surface electron accumulation on the Pt shell thickness. Figure 4 illustrates the differential charge densities in the presence of one additional electron as a function of the Pt shell thickness. As summarized in Table S4, the charge accumulation on the Pt surface follows the same thickness dependence as in the neutral state; however, 0.309 electrons can still be accumulated on the Pt surface as the thickness increases from one to four atomic layers. As such, charge separation can be promoted even when the Pt shells are thicker than four atomic layers. Therefore, TiO_2–Pd@Pt_{10} shows better charge separation than TiO_2–Pt (see Figure 2a–c).

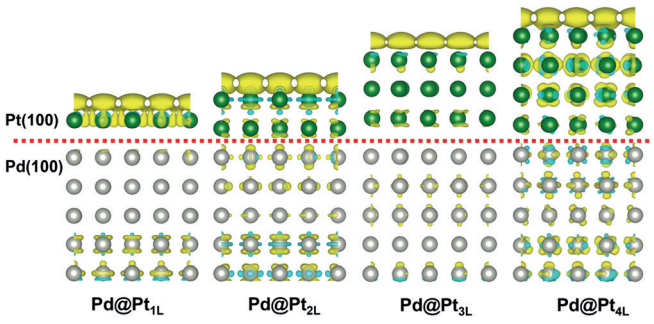

Figure 4. Differential charge density determined by first-principles simulations for the Pt(100) shells on Pd(100) substrates in the presence of one additional electron (subtracting the charges in the neutral case (Figure S15) from this system). The olive and cyan colors represent an increase and decrease in electron density, respectively. No other gradient colors were used to reflect the charge information. The isovalue chosen to plot the isosurfaces is 0.0004 e $Å^{-3}$.

Next, the question arose as to what impact the quasi-core–shell structures of the cocatalysts have on the water-splitting reaction. Aside from charge separation, surface reactions are another key step to photocatalysis. Pt is know to be the most active cocatalyst with the lowest activation energy for H_2 evolution.[4] Therefore, the adsorption of H_2O onto a Pt surface should be critical to photocatalytic water splitting.[21] Table S5 lists the H_2O adsorption energies of various Pt(100) surfaces obtained from first-principles simulations by altering the Pt shell thickness and substrate material. A comparison reveals three factors that may contribute to the adsorption of H_2O onto Pt surfaces.

First, the addition of photoexcited electrons enhances H_2O adsorption as indicated by the comparison of the neutral state with that with one additional electron. Second, the interfacial polarization that leads to the accumulation of electrons on the Pt surface should be capable of further improving the H_2O adsorption. As this polarization effect is absent in the case of bare Pt (e.g., Pt_{5L}@Pt_{4L}), the Pd@Pt quasi-core–shell cocatalysts can provide a more active surface for the water-splitting reaction than the bare Pt cocatalyst despite their similar Pt(100) surfaces. Third, although the effect from interfacial polarization slightly decays as the thickness of the Pt shell increases from one to four atomic layers in the presence of one additional electron, the lattice strain at the Pd–Pt interface would facilitate H_2O adsorption. A similar strain-induced effect has been observed in electrocatalysis.[20] As a result, the adsorption energy shows a volcano maximum at two to three atomic layers (see Table S5). Overall, the Pd@Pt quasi-core–shell cocatalysts (particularly those with atomic thickness) promote both charge separation and molecular reactions and are thus superior to Pt cocatalysts in photocatalytic water splitting.

In summary, we have designed atomically controlled Pd@Pt quasi-core–shell cocatalysts and deposited them on TiO_2 nanosheets. The well-designed cocatalysts play a dual role during photocatalytic water splitting, both of which are dependent on the Pt shell thickness: improving charge separation by promoting electron trapping with interfacial charge polarization, and enhancing H_2O adsorption onto the Pt surface by increasing the electron density and lattice strain. This approach, which reduces the amount of expensive Pt required while boosting the photocatalytic performance, represents a significant step towards the development of high-performance, low-cost photocatalysts.

Acknowledgements

This work was financially supported by the 973 Program (2014CB848900), the NSFC (21471141, 21473166, and 21473169), the Recruitment Program of Global Experts, the CAS Hundred Talent Program, and the Fundamental

Research Funds for the Central Universities (WK2060190025, WK2310000035, and WK2060030014).

Keywords: cocatalysts · core–shell nanoparticles · photocatalysis · platinum · water splitting

How to cite: *Angew. Chem. Int. Ed.* **2015**, *54*, 14810–14814
Angew. Chem. **2015**, *127*, 15023–15027

[1] A. Fujishima, K. Honda, *Nature* **1972**, *238*, 37.
[2] R. Asahi, T. Morikawa, T. Ohwaki, K. Aoki, Y. Taga, *Science* **2001**, *293*, 269.
[3] K. Maeda, K. Teramura, D. L. Lu, T. Takata, N. Saito, Y. Inoue, K. Domen, *Nature* **2006**, *440*, 295.
[4] J. Yang, D. Wang, H. Han, C. Li, *Acc. Chem. Res.* **2013**, *46*, 1900.
[5] A. L. Linsebigler, G. Lu, J. T. Yates, Jr., *Chem. Rev.* **1995**, *95*, 735.
[6] S. Bai, J. Jiang, Q. Zhang, Y. Xiong, *Chem. Soc. Rev.* **2015**, *44*, 2893.
[7] S. Bai, C. Wang, M. Deng, M. Gong, Y. Bai, J. Jiang, Y. Xiong, *Angew. Chem. Int. Ed.* **2014**, *53*, 12120; *Angew. Chem.* **2014**, *126*, 12316.
[8] X. Han, Q. Kuang, M. Jin, Z. Xie, L. Zheng, *J. Am. Chem. Soc.* **2009**, *131*, 3152.
[9] B. Li, R. Long, X. Zhong, Y. Bai, Z. Zhu, X. Zhang, M. Zhi, J. He, C. Wang, Z. Y. Li, Y. Xiong, *Small* **2012**, *8*, 1710.
[10] S. Xie, S. I. Choi, N. Lu, L. T. Roling, J. A. Herron, L. Zhang, J. Park, J. Wang, M. J. Kim, Z. Xie, M. Mavrikakis, Y. Xia, *Nano Lett.* **2014**, *14*, 3570.
[11] X. Wang, S. I. Choi, L. T. Roling, M. Luo, C. Ma, L. Zhang, M. Chi, J. Liu, Z. Xie, J. A. Herron, M. Mavrikakis, Y. Xia, *Nat. Commun.* **2015**, *6*, 7594.
[12] Y. Yang, J. Liu, Z. W. Fu, D. Qin, *J. Am. Chem. Soc.* **2014**, *136*, 8153.
[13] J. Bisquert, A. Zaban, M. Greenshtein, I. Mora-Seró, *J. Am. Chem. Soc.* **2004**, *126*, 13550.
[14] J. S. DuChene, B. C. Sweeny, A. C. Johnston-Peck, D. Su, E. A. Stach, W. D. Wei, *Angew. Chem. Int. Ed.* **2014**, *53*, 7887; *Angew. Chem.* **2014**, *126*, 8021.
[15] Y. C. Pu, G. Wang, K. D. Chang, Y. Ling, Y. K. Lin, B. C. Fitzmorris, C. M. Liu, X. Lu, Y. Tong, J. Z. Zhang, Y. J. Tsu, Y. Li, *Nano Lett.* **2013**, *13*, 3817.
[16] G. Kresse, J. Furthmüller, *Phys. Rev. B* **1996**, *54*, 11169.
[17] F. A. Cotton, G. Wilkinson, C. A. Murillo, M. Bochmann, *Advanced Inorganic Chemistry*, 6th ed., Wiley, New York, **1999**.
[18] J. Lu, K. B. Low, Y. Lei, J. A. Libera, A. Nicholls, P. C. Stair, J. W. Elam, *Nat. Commun.* **2014**, *5*, 3264.
[19] B. Y. Xia, B. Wang, H. B. Wu, Z. Liu, X. Wang, X. W. Lou, *J. Mater. Chem.* **2012**, *22*, 16499.
[20] L. Yang, M. B. Vukmirovic, D. Su, K. Sasaki, J. A. Herron, M. Marrikakis, S. Liao, R. R. Adzic, *J. Phys. Chem. C* **2013**, *117*, 1748.
[21] D. Donadio, L. M. Ghiringhelli, L. D. Site, *J. Am. Chem. Soc.* **2012**, *134*, 19217.

Received: August 27, 2015
Published online: October 14, 2015

